RESEARCH ARTICLE

NEURAL CIRCUITS

Prefrontal cortical regulation of brainwide circuit dynamics and reward-related behavior

Emily A. Ferenczi,[1,2]* Kelly A. Zalocusky,[1,2]* Conor Liston,[3]* Logan Grosenick,[1,2] Melissa R. Warden,[4] Debha Amatya,[1] Kiefer Katovich,[5] Hershel Mehta,[5] Brian Patenaude,[6] Charu Ramakrishnan,[1] Paul Kalanithi,[7] Amit Etkin,[6] Brian Knutson,[5] Gary H. Glover,[8] Karl Deisseroth[1,4,9]†

Motivation for reward drives adaptive behaviors, whereas impairment of reward perception and experience (anhedonia) can contribute to psychiatric diseases, including depression and schizophrenia. We sought to test the hypothesis that the medial prefrontal cortex (mPFC) controls interactions among specific subcortical regions that govern hedonic responses. By using optogenetic functional magnetic resonance imaging to locally manipulate but globally visualize neural activity in rats, we found that dopamine neuron stimulation drives striatal activity, whereas locally increased mPFC excitability reduces this striatal response and inhibits the behavioral drive for dopaminergic stimulation. This chronic mPFC overactivity also stably suppresses natural reward-motivated behaviors and induces specific new brainwide functional interactions, which predict the degree of anhedonia in individuals. These findings describe a mechanism by which mPFC modulates expression of reward-seeking behavior, by regulating the dynamical interactions between specific distant subcortical regions.

The drive to pursue and consume rewards is highly conserved across species (*1*). Subcortical neuromodulatory systems, including midbrain dopaminergic projections, play a central role in predicting and signaling the availability of rewards (*2*–*5*). Anhedonia represents a core symptom of depression but also characterizes other neuropsychiatric disorders, including schizophrenia, suggesting the possibility of shared neural substrates (*6*). Although the underlying cause of anhedonia remains unknown, a number of hypotheses exist, including cortically driven dysregulation of subcortical circuits (*7*–*10*). Imaging studies have detected elevated metabolic activity in the mPFC of human patients suffering from depression (*11*); this type of brain activity is correlated with anhedonic symptoms (*12*–*16*). In particular, the subgenual cingulate gyrus of the medial prefrontal cortex (mPFC) is a therapeutic target for deep brain stimulation in refractory depression, and treatment has been associated with normalization of this localized hyperactivity, alongside patient reports of renewed interest in rewarding aspects of life (*11*, *17*, *18*). By combining optogenetics with functional magnetic resonance imaging (fMRI), we sought to test the hypothesis that the mPFC exerts causal top-down control over the interaction of specific subcortical regions governing dopamine-driven reward behavior, with important implications for anhedonia.

Although human fMRI experiments have resolved activity patterns in distinct subregions of the brain that respond to reward anticipation and experience (*19*, *20*), the causal relationships between neuronal activity in reward-related circuits and brainwide blood oxygen level–dependent (BOLD) patterns have yet to be established. In optogenetic fMRI (ofMRI), light-responsive regulators of transmembrane ion conductance (*21*) are introduced into target cell populations and controlled by focal pulses of light to assess the causal impact of the targeted circuit elements on local and global fMRI responses. We developed and extended this technique to scanning of awake rats and included a number of optogenetic tools specifically suited to our experimental questions.

We began by mapping the brainwide BOLD response to optogenetic stimulation of dopamine neurons in transgenic tyrosine hydroxylase driver (TH-Cre) rats, using an excitatory channelrhodopsin (ChR2 His^{134}→Arg^{134}, hereafter referred to as ChR2). Next, we tested effects of a similarly targeted inhibitory opsin, the enhanced *Natromonas* halorhodopsin (eNpHR3.0) (*22*). We hypothesized that such inhibition of dopamine neurons would reduce BOLD activity in downstream regions, although it is unknown whether tonic dopamine levels would be sufficient to allow detection of a downward modulation in BOLD. Furthermore, the expected direction of the BOLD response is a matter of debate, given the functional heterogeneity of dopamine receptors.

Finally, we assessed the influence of mPFC excitability over this subcortical dopaminergic reward signaling. Altered excitability in the mPFC has been correlated with anhedonic behaviors in human patients and mice (*23*), and there is a growing body of literature characterizing altered resting-state BOLD correlations in patients with psychiatric disease (*24*). Nevertheless, it is still unclear whether and to what extent local changes in prefrontal cortex activity might propagate to distant brain regions to modulate reward-related signals. To address these questions, we used the stabilized step-function opsin (SSFO), a double-mutant excitatory ChR2 (Cys^{128}→Ser^{128}, Asp^{156}→Ala^{156}) engineered to have slow off-kinetics (rate of channel closure τ_{off} ~ 30 min) (*23*). Upon activation by blue light, SSFO causes stable subthreshold depolarization of cell bodies, sensitizing neurons to synaptic input. The resulting elevated excitability of targeted cells (*23*, *25*) outlasts the light pulse, permitting extended-duration shifts in neural excitability and moderate asynchronous increases in neural firing. In milliseconds, SSFO can also be switched off by a pulse of yellow light; this feature is essential for repetitive stimulation in fMRI experiments. Additionally, the transient and minimal light requirements of SSFO decrease the potential for tissue heating (which could cause an artifact in fMRI BOLD studies) (*26*). To directly test the hypothesis that mPFC modulates dopaminergic reward signaling in the striatum, we devised dual-stimulation experiments, combining mPFC SSFO stimulation with dopaminergic midbrain stimulation by using the spectrally shifted excitatory tool $C1V1_{TT}$ [a red-shifted hybrid (*23*, *27*) between *Chlamydomonas* and *Volvox* channelrhodopsins], permitting the assessment of interaction between two distinct cell populations.

Results

Awake ofMRI

Because reward anticipation and experience involve varying states of arousal, and because anesthesia dampens BOLD activity, assessment of the neural activity of awake and alert animals was critical for the collection of behaviorally relevant brainwide signals (*28*). We therefore established protocols for ofMRI in the awake rat, with careful animal habituation and monitoring, permitting the imaging of brain networks uncontaminated by anesthesia or excessive subject movement. Animals were habituated in a mock MRI environment before scanning (Fig. 1A), and respiratory rate and head motion were monitored during scanning (Fig. 1, B to D). Compared with anesthetized protocols, our protocol enhanced the detection of evoked changes in BOLD activity (fig. S1 and table S1). In addition to scanning fluorophore-only (virus-injected, fiber-implanted,

[1]Department of Bioengineering, Stanford University, Stanford, CA 94305, USA. [2]Neurosciences Program, Stanford University, Stanford, CA 94305, USA. [3]Brain Mind Research Institute, Weill Cornell Medical College, New York, NY 10065, USA. [4]Department of Neurobiology and Behavior, Cornell University, Ithaca, NY 14853, USA. [5]Department of Psychology, Stanford University, Stanford, CA 94305, USA. [6]Department of Psychiatry and Behavioral Sciences, Stanford University, Stanford, CA 94305, USA. [7]Department of Neurosurgery, Stanford University, Stanford, CA 94305, USA. [8]Department of Radiology, Stanford University, Stanford, CA, 94305, USA. [9]Howard Hughes Medical Institute, Stanford University, Stanford, CA, 94305, USA.
*These authors contributed equally to this work.
†Corresponding author. E-mail: deissero@stanford.edu

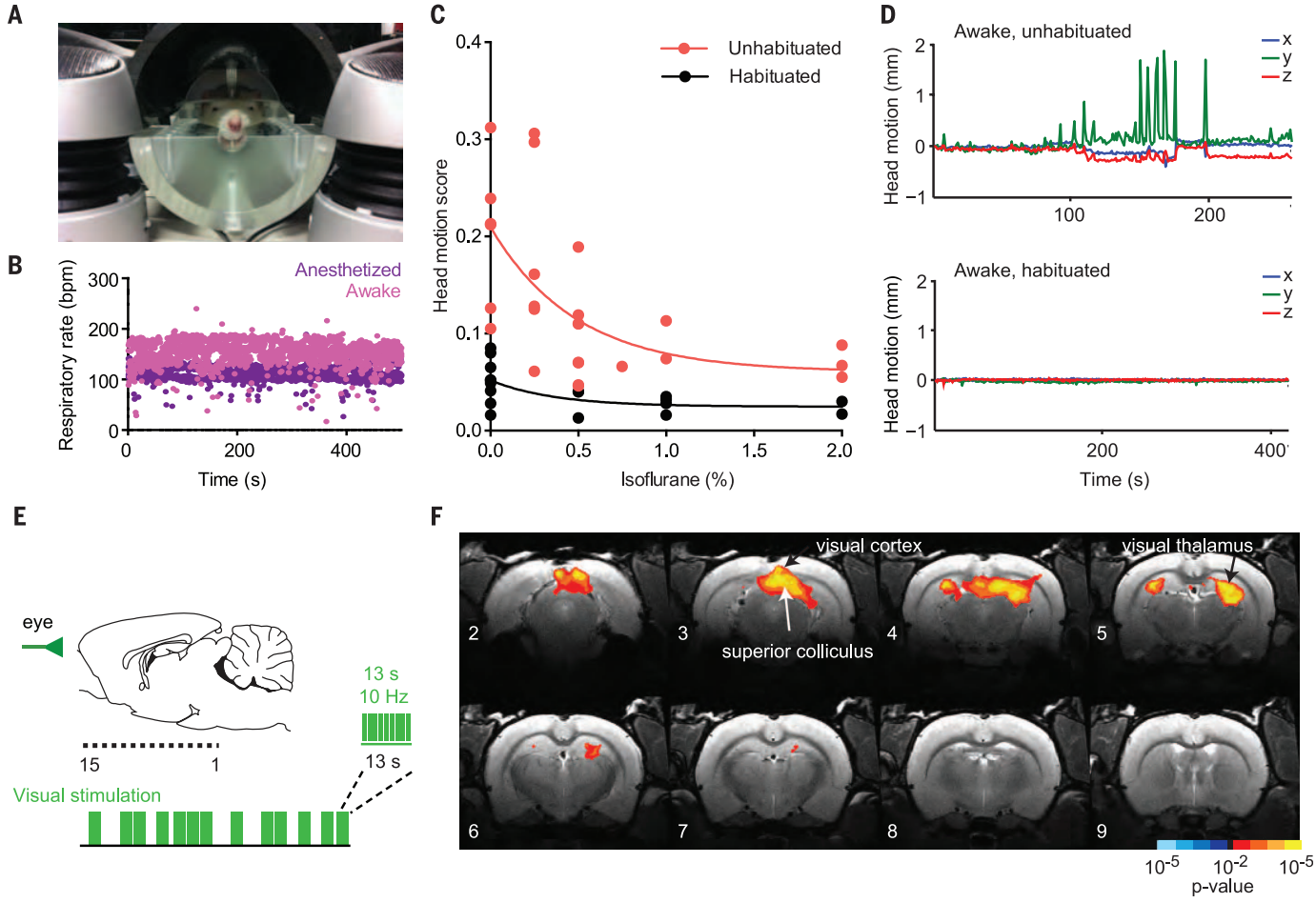

Fig. 1. Optogenetic functional MRI (ofMRI) in awake rats. (**A**) MRI simulation environment for rodent habituation to the scanning procedure. (**B**) Example of respiratory rate monitoring [bpm, breaths per minute; n = 1 rat; eight sequential scans, four anesthetized (1 to 2% isoflurane) and four awake (0% isoflurane)]. (**C**) Effect of habituation on head motion during scanning, as a function of anesthesia depth (n = 2 rats). Head motion score is the root mean square of head translation in three dimensions over the course of a scan. (**D**) Example head motion plots (head translation in three dimensions, calculated as shifts in the center of mass of all voxels in the image over the course of a single scan) for an unhabituated (top) and a habituated (bottom) subject. The unhabituated scan was aborted early. (**E**) Visual stimulation during fMRI. A sagittal view of the brain indicates the location of MRI images from anterior (image 15) to posterior (image 1). The schematic illustrates event-related stimulation design. (**F**) Z-score map of BOLD activity in visual brain regions in response to visual stimulation in control subjects (n = 5 rats, 20 runs). For this figure and all subsequent statistical maps, maps were thresholded at $P < 0.05$ (corrected) [$K > 5$ functional voxels (80 transformed voxels), uncorrected $P < 0.01$]. Gradations in color (e.g., red-orange-yellow) indicate incremental P-value thresholds of one order of magnitude.

no opsin) negative-control subjects [yellow fluorescent protein (YFP) controls], we incorporated a nonoptogenetic visual stimulus as a positive control into our standard fMRI stimulation protocol, in which moderate green light (bursts of 13 s, 10 Hz, 20-ms pulse width, ~0.5 mW) was flashed in front of the eye in a pseudorandomly ordered event-related sequence (Fig. 1E). This stimulus evoked predictable and consistent BOLD activity in subcortical visual regions (superior colliculus, lateral geniculate nucleus) (Fig. 1F).

Brainwide mapping of a dopamine neuron–driven rewarded state

We next investigated how activity in midbrain dopamine neurons affects BOLD activity patterns in dopamine terminal regions (*20*). Because optogenetic control of dopamine neurons has been shown to drive reward-seeking behavior in rodents (*29*, *30*), we predicted that phasic activation of midbrain dopamine neurons would increase striatal BOLD activity by driving synaptic input to the region (*31*), and the response in ventral striatum would be closely correlated with reward-seeking behavior.

We expressed ChR2 fused with YFP in midbrain dopamine neurons by unilaterally injecting a Cre-dependent construct into the right midbrain of tyrosine-hydroxylase TH-Cre transgenic Long-Evans rats (*30*) (Fig. 2A). Specific expression was confirmed by colocalization of YFP with anti-TH staining in confocal images (Fig. 2A). We performed optogenetic stimulation of midbrain dopaminergic neurons in a 7-T small-animal scanner. Blue light pulses were delivered to the midbrain of awake, habituated rats [we used a physiologically relevant in magnitude, event-related stimulation design (phasic 2-s bursts of 20-Hz blue light pulses, 10-ms pulse width, minimum of 11-s recovery time after each stimulation burst) interleaved with the nonoptogenetic visual stimulus described above (Fig. 2B)]. We chose a 2-s burst duration because initial dose-response experiments indicated that this duration was more effective at driving reward-seeking behavior (fig. S2A) and reliable striatal BOLD activity (fig. S2, B and C) compared with shorter burst durations and was also within a previously validated physiological burst-duration range for ventral tegmental area (VTA) neurons (*32*). Unilateral ChR2 stimulation of the midbrain evoked robust, largely ipsilateral increases in BOLD activity in the dorsal and ventral striatum (Fig. 2G), as well as increases in other brain regions, including the retrosplenial cortex and thalamus (Fig. 2C). These widespread changes in BOLD activity were not observed in fluorophore-only (no opsin) YFP-control subjects (Fig. 2, D and H), despite robust activity increases during visual stimulation (Fig. 2, E and F), and the difference in optogenetic response was significant between the ChR2 and YFP-control groups (fig. S3, A and B, and table S2).

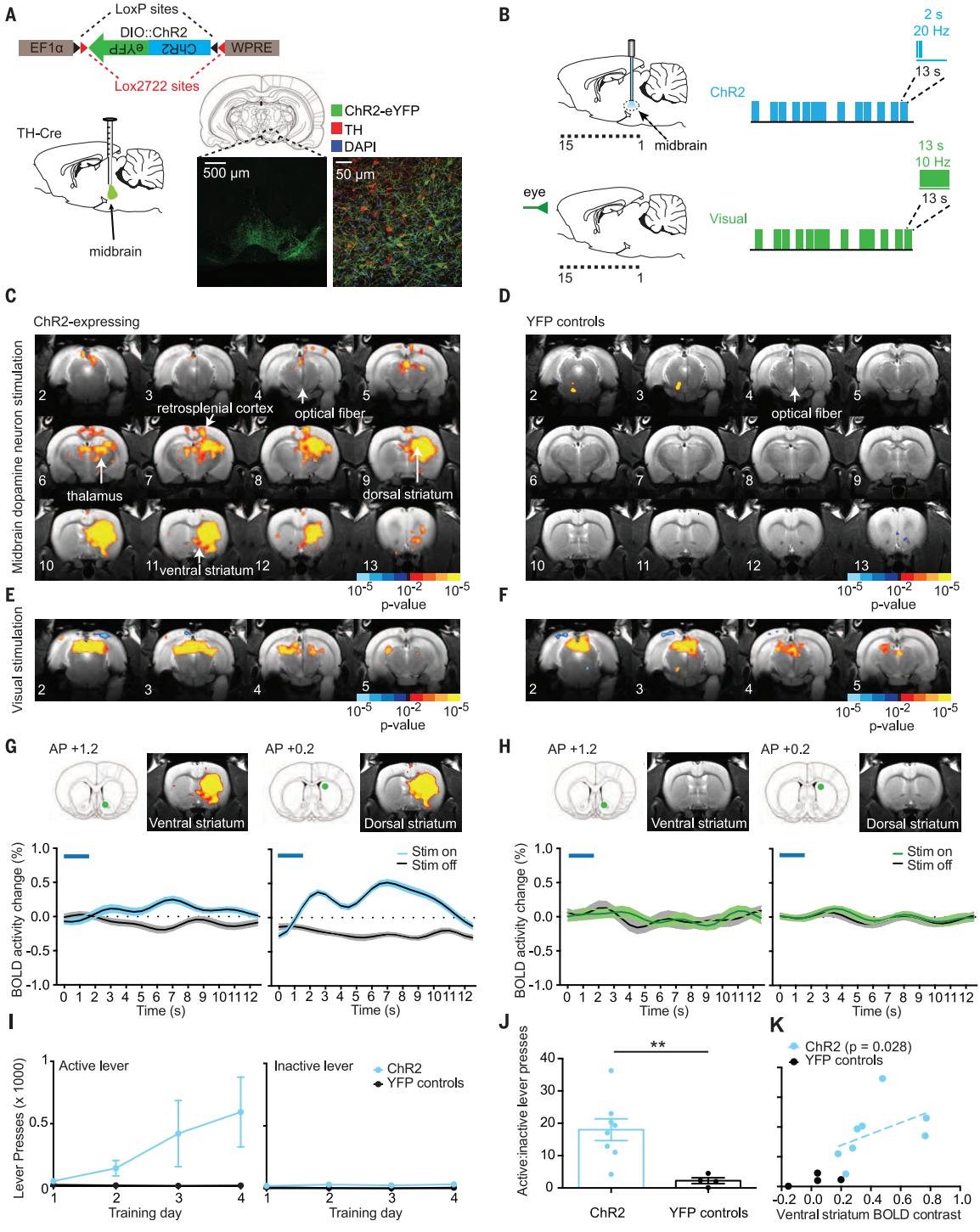

Fig. 2. Influence of midbrain optogenetic dopamine stimulation on brain-wide BOLD activity and behavior. (**A**) Schematic of Cre-dependent ChR2 construct and sagittal view of injection site in the midbrain. Confocal images demonstrate ChR2 expression in dopaminergic neurons in the midbrain. Green, ChR2-YFP; red, tyrosine hydroxylase (TH); blue, 4′,6-diamidino-2-phenylindole (DAPI). (**B**) Schematic of event-related design for midbrain ChR2 stimulation and visual stimulation. (**C**) *Z*-score map of BOLD activity in response to ChR2 stimulation of midbrain dopamine neurons (n = 8 rats, 34 runs). (**D**) *Z*-score map for YFP-control subjects in response to blue light stimulation in the midbrain (n = 4 rats, 21 runs). (**E**) *Z*-score maps for ChR2-expressing subjects (n = 8 rats, 34 runs) and (**F**) YFP-control subjects (n = 4 rats, 21 runs) in response to visual stimulation. (**G**) Average ChR2 stimulation–locked BOLD activity time courses in the ventral and dorsal striatum for ChR2-expressing subjects (n = 8 rats, 34 runs) and (**H**) YFP-control subjects (n = 4 rats, 16 runs). Mean and SEM (n = number of runs) are shown. Timing of light delivery is indicated by the blue lines above the plots. Regions of interest (ROIs) used for time-course extraction are indicated by green dots on atlas images above plots. (**I**) Active and inactive lever presses as a function of training day for ChR2-expressing (n = 8) and YFP-control (n = 4) rats. (**J**) Active-to-inactive lever press ratio on the final day of training for ChR2 and YFP rats (two-tailed Mann-Whitney *U* test: sum of ranks = 68, 11; U = 1; $^{**}P$ = 0.0081). (**K**) Relationship between BOLD activity contrast in the ventral striatum and active-to-inactive lever press ratio for ChR2-expressing subjects (n = 8 rats, Spearman ρ = 0.78, P = 0.028) and YFP-expressing subjects (n = 4 rats).

Visualization of the dynamic influence of optogenetic dopamine stimulation on downstream BOLD activity through stimulation-locked averaged time courses suggested that striatal BOLD activity exhibited a double-peaked profile, particularly in the dorsal striatum (Fig. 2G and fig. S3C). The early response, which peaked 2 to 3 s after the onset of stimulation, with a fast decline, was tightly correlated in magnitude with a second later response (fig. S3D). We suspected that this prompt response resulted directly from vascular inflow to activated regions (providing new, unsaturated spins to blood vessel–containing regions, enhancing signal independently of blood oxygenation level), which we were able to detect because of our fast sampling rate [repetition time (TR) = 0.5 s] (*33*). There was no response to optogenetic stimulation in fluorophore-only YFP-control subjects (Fig. 2H).

Operant chamber behavioral testing confirmed the rewarding nature of optogenetic stimulation of midbrain dopaminergic neurons. ChR2-expressing but not YFP-control rats reliably chose to press a lever to deliver blue light stimulation to the midbrain (active lever), as opposed to a lever that delivered no light (inactive lever) (Fig. 2, I and J). We noted a significant correlation between an individual rat's preference for the active lever over the inactive lever in the operant chamber and the change in BOLD activity in the rat's ventral striatum during ChR2 stimulation in the scanner (Fig. 2K). A similar relation was observed in the dorsal striatum (fig. S3, E and F). Significant correlations were not observed for the total number of lever presses, suggesting that the BOLD activity change was associated with lever selection preference rather than overall motor activity (fig. S3, G and H). Striatal BOLD activity was also influenced by the medial-lateral position of the optical fiber within the VTA (fig. S4), with more lateral positioning associated with stronger BOLD responses in both the dorsal and ventral striatum.

Dopamine neuron–driven BOLD activity patterns require dopamine receptor activation

To better understand the mechanisms underlying BOLD activity patterns driven by activity in dopamine neurons, we next tested whether these BOLD patterns required dopamine receptor activation. In four rats, we performed a series of longitudinal pharmacological experiments consisting of a baseline scan (no pharmacological agents), followed ~24 hours later by a scan in which a cocktail of dopamine D1 receptor and D2 receptor antagonists was administered intraperitoneally immediately before acquisition of functional images, followed by a washout scan (with intraperitoneal injection of saline/dimethyl sulfoxide vehicle control) performed 24 to 48 hours after drug administration to allow sufficient time for drug elimination (*34*, *35*) (Fig. 3, A to C). We observed robust increases in striatal BOLD activity in response to dopamine neuron stimulation at baseline (Fig. 3A). Administration of the dopaminergic antagonists (Fig. 3, B and D to F) significantly reduced these responses. Increases in BOLD activity returned during the washout phase (Fig. 3, C to E; fig. S5; and tables S3 and S4). The ability of the visual stimulus to increase BOLD activity in visual processing circuits remained strong. In fact, it was stronger during D1 and D2 receptor antagonist administration than at baseline and washout, eliminating the possibility that dopamine antagonism abolished all BOLD activity throughout the brain (Fig. 3, A to E) and supporting previous research suggesting that tonic dopamine may play a role in modulating visual processing (*36*–*38*).

These findings were confirmed by a model-free support vector machine classification analysis with recursive feature elimination (SVM-RFE) (*39*) (fig. S6). At baseline, SVM-RFE classified midbrain stimulation versus no stimulation with 82 to 84% accuracy, but accuracy level fell to 63 to 66% for scans acquired after administration of D1 and D2 receptor antagonists and to chance classification rates (~50 to 55%) for YFP-control subjects (fig. S6A). SVM-RFE classified visual stimulation versus no stimulation with 72 to 80% accuracy at baseline and for YFP controls, and the accuracy level increased to 85 to 86% for scans acquired after D1 and D2 receptor antagonist administration (fig. S6B). When features from these optimal classifiers were back-projected onto brain volumes over time, the features were located in the striatum for optogenetic midbrain stimulation and in the visual midbrain and thalamus for visual stimulation, confirming the magnitude and spatial localization of the BOLD activity and its responsiveness to modulation by pharmacological agents during two different types of stimulation.

Optogenetic inhibition of dopamine neurons decreases BOLD activity in divergent brain regions

We wondered whether the silencing of dopamine neurons would also influence BOLD activity. We predicted that because dopamine neurons exhibit tonic activity (*40*), which can be depressed by reward omission (*41*), optogenetic inhibition might decrease BOLD activity in brain regions that are responsive to this tonic input. We expressed the yellow light–activated halorhodopsin eNpHR3.0 (*22*) via a Cre-dependent construct in the midbrain of TH-Cre transgenic rats and histologically confirmed colocalization of TH and eNpHR3.0 expression (fig. S7A). A real-time place preference test revealed that the majority of rats spent significantly less time in the chamber in which they received inhibition of midbrain dopamine neurons (fig. S7B), but midbrain inhibition had little influence on locomotor behavior (fig. S7B). In the MRI scanner, yellow light pulses (590 nm) were delivered to the midbrain with the same event-related design previously used for stimulation, with either 2- or 10-s continuous light pulses (rather than 20-Hz pulses), in parallel with visual stimulation as before (fig. S7, C and F). We observed decreased BOLD activity in the hypothalamus and dorsal striatum in response to the eNpHR3.0 manipulation (fig. S7, D and E), and this result was more pronounced for 10-s inhibition than for 2-s inhibition (fig. S7, G and H, and fig. S2B). Thus, this finding confirms that neural silencing can reduce BOLD activity in a dose-dependent manner (fig. S2, B and C) but in a slightly different spatial pattern from that elicited by phasic activation.

Elevated excitability of the mPFC suppresses natural reward-related behavior

Having characterized brainwide BOLD activity patterns corresponding to a dopamine neuron–driven rewarded state, we next sought to investigate how these signals might be modulated by top-down cortical glutamatergic input, which has been implicated in physiological reward-seeking behaviors (*42*) and pathological anhedonic states (*23*). Neuroimaging studies indicate that elevated metabolic activity in the ventromedial prefrontal cortex is associated with anhedonic symptoms in depression (*11*–*16*), and normalization of prefrontal hyperactivity is associated with renewed interest in rewarding activities (*11*, *17*, *18*). We therefore chose an optogenetic stimulation method (SSFO) that would not drive synchronous elevation in cortical firing but would instead produce an asynchronous enhancement of excitability (*23*) to most accurately re-create the proposed human pathophysiology. We hypothesized that although this manipulation may favor local BOLD activity within the mPFC, the wide-reaching projections of the mPFC would exert a subtler, more modulatory effect through changes in coordination of activity between brain regions (*43*) rather than through directly evoking downstream BOLD activity. Because the cortex is thought to sculpt subcortical activity through feed-forward inhibition via fast-spiking interneurons (*44*), we suspected that elevated cortical excitability might suppress the response of the striatum to dopaminergic signals from the midbrain.

Using the Ca^{2+}/calmodulin kinase IIα (CaMKIIα) promoter, we expressed an optogenetic neural sensitizer (SSFO) to specifically drive asynchronous neural excitability, targeting predominantly excitatory glutamatergic pyramidal neurons in the mPFC of wild-type Sprague-Dawley rats (*45*, *46*) (Fig. 4A). We used in vivo optrode recordings of multiunit activity to confirm the ability of SSFO to increase the excitability of mPFC in response to blue light, as well as the reversibility of this effect with yellow light (Fig. 4B). We also ensured that this excitability increase was asynchronous across neurons as expected, using in vivo multielectrode-array single-unit recordings in awake rats (fig. S8, A to E).

We next performed SSFO optogenetic stimulation experiments in awake rats during fMRI scanning. Rats received stimulation of the mPFC in an event-related design, using a 2-s continuous blue light pulse to activate SSFO (or sham-activate a YFP control) for a total of 10 s. This was followed by deactivation with a 3-s yellow light pulse (Fig. 4C), again interleaved with visual

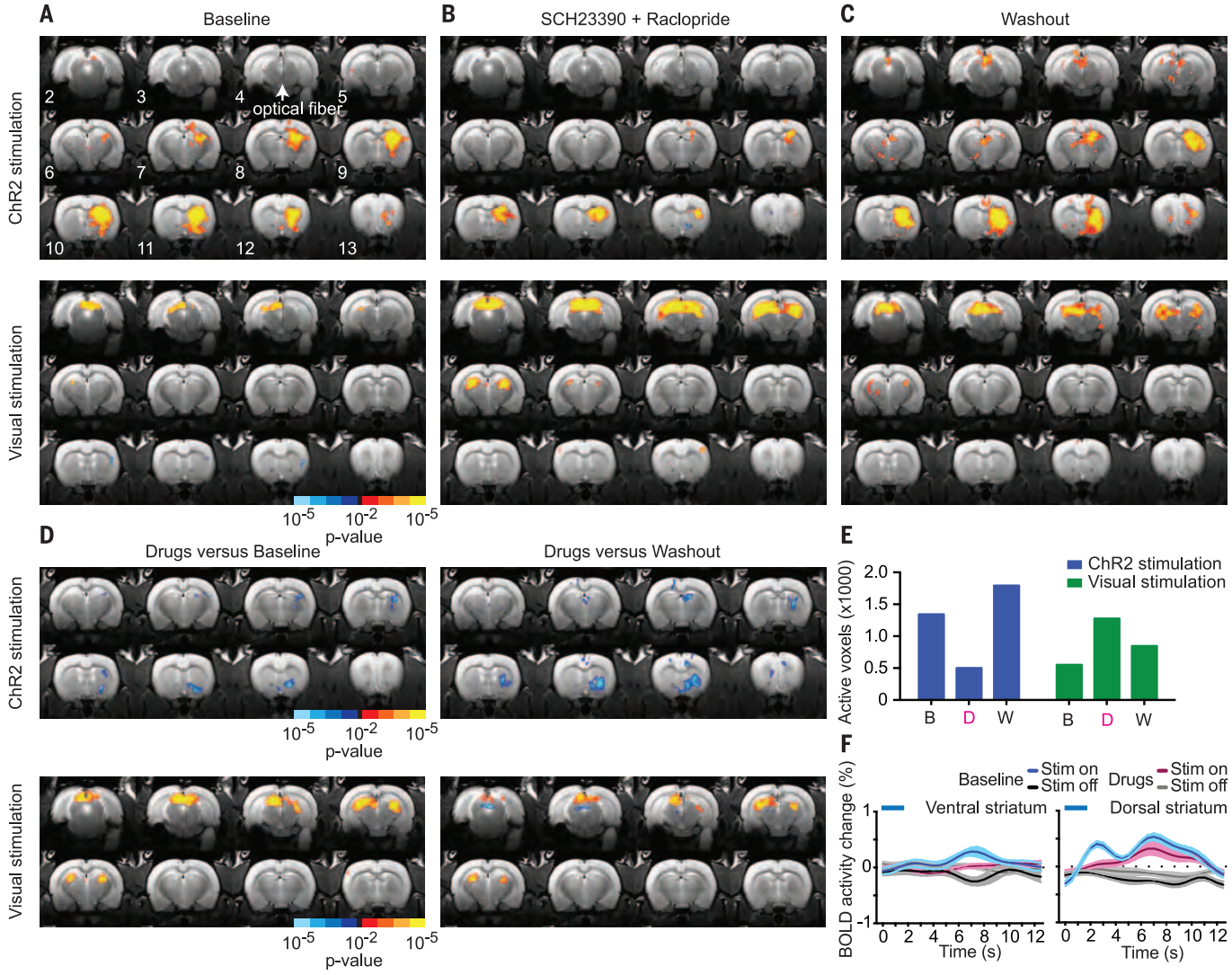

Fig. 3. Sensitivity of brainwide ofMRI BOLD patterns to dopamine receptor pharmacological inhibition. (**A** to **C**) Sequential pharmacological experiments in ChR2-expressing TH-cre rats undergoing ChR2 stimulation of midbrain dopamine neurons (top) and visual stimulation (bottom). (A) Baseline scan (no drugs or vehicle administered, n = 4 rats, 16 runs). (B) Drug scan: systemic (intraperitoneal) administration of D1 (SCH23390, 0.6 mg/kg) and D2 (raclopride, 0.3 mg/kg) dopamine receptor antagonists immediately before acquisition of functional scans (n = 4 rats, 22 runs). (C) Vehicle control washout scan: 48 to 24 hours after drug administration (n = 4 rats, 18 runs). (**D**) Statistical comparison between drug-versus-baseline and drug-versus-washout conditions for ChR2 and visual stimulation. (**E**) Total number of activated voxels in response to ChR2 and visual stimulation under each pharmacological condition. B, baseline; D, drug; W, washout. (**F**) Average stimulation-locked BOLD activity time courses in the ventral and dorsal striatum in response to ChR2 stimulation of midbrain dopamine neurons at baseline (n = 4 rats, 16 runs) in the presence of systemic D1 and D2 receptor antagonists (n = 4 rats, 22 runs). Mean and SEM (n = number of runs) are shown.

stimulation bursts (13 s of 10-Hz green light flashes), to serve as a natural sensory positive control (Fig. 4F). During SSFO stimulation, we observed increased BOLD activity at the optical fiber site [with only limited extension to known nearby projection regions (*47*), consistent with the desired subtle and focal nature of the SSFO-mediated optogenetic manipulation] in SSFO-expressing subjects (Fig. 4D) but not in YFP controls (Fig. 4E), with a significant difference in optogenetic mPFC activation between the two groups (fig. S9A and table S5) despite a similar response to visual stimulation (Fig. 4, G and H, and fig. S9B).

On the basis of human neuroimaging studies, we predicted that this modulation of mPFC excitability would reduce the expression of reward-seeking behavior (*15*, *16*). We employed two well-established appetitive assays: the sucrose preference test (*32*, *48*–*50*) and the social interaction test (*51*). We used a chronic (12-day) sucrose preference test (Fig. 4I) in which rats' preference for a 1% sucrose solution relative to plain water was measured daily. SSFO-expressing rats showed a mild but consistent and reversible reduction in sucrose preference only during days when light-stimulation was delivered. In contrast, YFP-control rats maintained a preference for sucrose (~90%) over the entire testing period (Fig. 4J). Plain water consumption was largely unchanged (Fig. 4K).

In the social interaction test (Fig. 4L), SSFO-expressing rats demonstrated a reversible reduction in social interaction after 3 days of light stimulation, whereas YFP-control rats showed a similar level of interaction across all three tests (Fig. 4M). At the start of the test, SSFO-expressing rats still recognized and explored the juvenile rat to an extent comparable to their YFP-expressing counterparts, but with chronic light stimulation, this engagement diminished more rapidly in SSFO-expressing rats compared with YFP-expressing rats (Fig. 4P). We did not observe any light-mediated effects on novel object exploration, as rats in both groups exhibited initial interest in the novel object, which then abated (Fig. 4N and fig. S10B). We also did not observe any differences in locomotor behavior, consistent with previous studies of mice (Fig. 4O) (*23*).

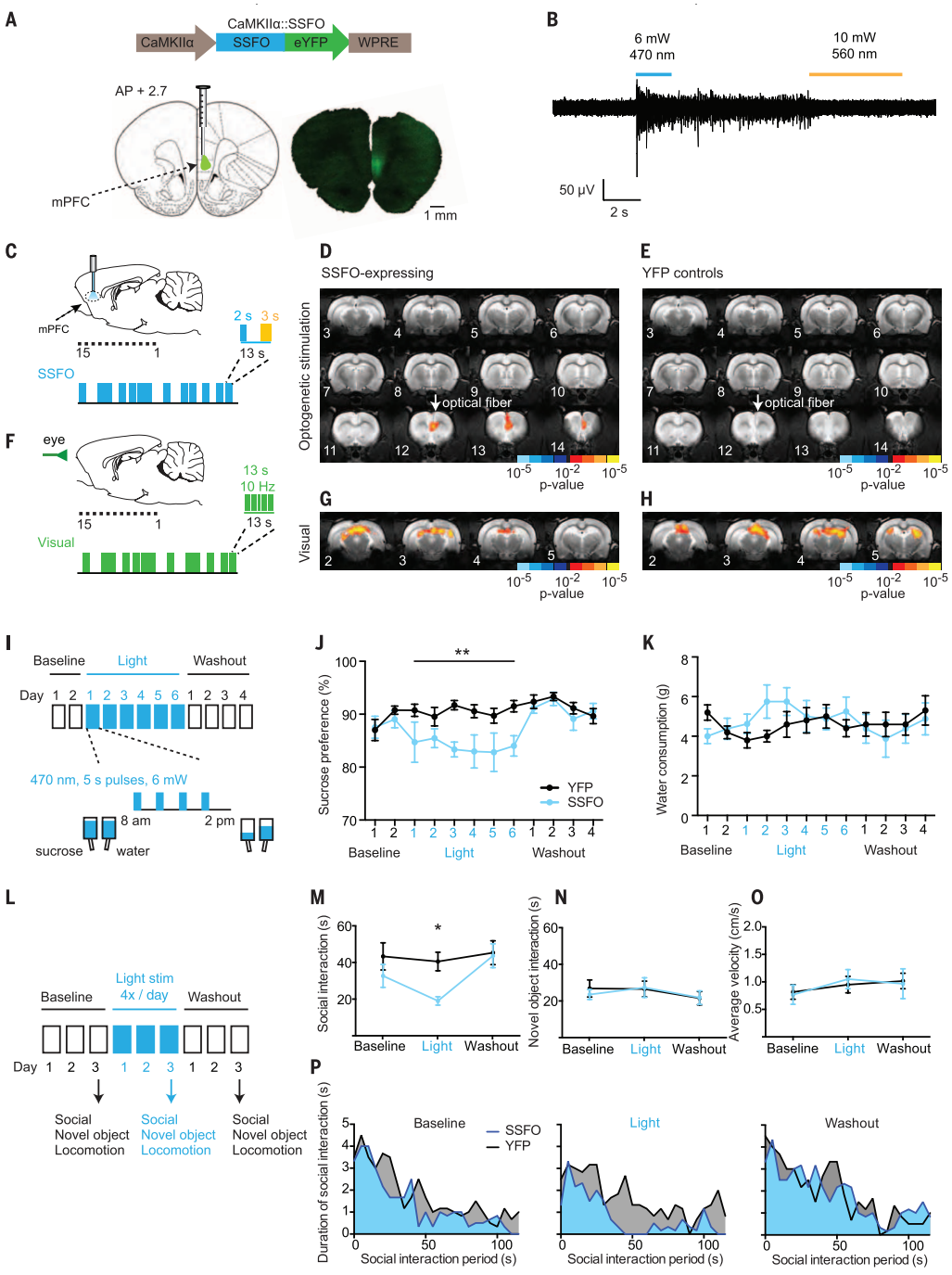

Fig. 4. Prefrontal cortical excitability modulation of multiple natural reward-related behaviors. (**A**) Schematic of the optogenetic construct CKIIα-SSFO-eYFP. Confocal image of SSFO-YFP expression in the mPFC. WPRE, woodchuck hepatitis virus posttranscriptional regulatory element. (**B**) Example of multiunit in vivo anesthetized optrode recording of SSFO stimulation in the mPFC, terminated by yellow light. (**C**) Event-related SSFO stimulation of the mPFC during fMRI scanning (optical fiber positioned in mPFC image 12). (**D**) Brain-wide *Z*-score map of BOLD activity in response to SSFO stimulation of the mPFC in SSFO-expressing subjects (n = 6 rats, 17 runs) and (**E**) YFP-control subjects (n = 5 rats, 20 runs). (**F**) Event-related visual stimulation. (**G**) *Z*-score map in response to visual stimulation in SSFO-expressing subjects (n = 6 rats, 17 runs) and (**H**) YFP-control subjects (n = 5 rats, 20 runs). (**I**) Sucrose preference testing paradigm. (**J**) Sucrose preference across test days for SSFO-expressing subjects (blue, n = 8 rats) and YFP controls (black, n = 10 rats). Mean and SEM are shown. We found a significant interaction between group and test day [$F_{11,176}$ = 2.555, $^{**}P$ = 0.0051, two-way repeated measures analysis of variance (ANOVA)], with significant differences between SSFO and YFP-control groups on days 3, 4, and 6 of light stimulation (P < 0.05, Sidak's multiple comparisons test). (**K**) Plain water consumption across test days for SSFO-expressing subjects (blue, n = 8 rats) and YFP-controls (black, n = 10 rats). Mean and SEM are shown. We found no significant difference between SSFO-expressing and YFP-control groups after multiple comparison testing. (**L**) Social interaction test paradigm. (**M** to **O**) Total duration of social interaction, novel object interaction, and mean velocity are compared across the three test days (n = 6 rats for SSFO social behavior, n = 5 for novel object and velocity, and n = 6 for YFP). We found a significant main effect of light ($F_{2,20}$ = 5.470, $^{*}P$ = 0.0127, two-way repeated measures ANOVA), with a significant difference between SSFO and YFP-control groups only on the light-stimulation day (P < 0.05, Sidak's multiple comparisons test). (**P**) Social investigation (in 5-s bins) over the course of the interaction period. Shaded regions indicate the mean across all rats.

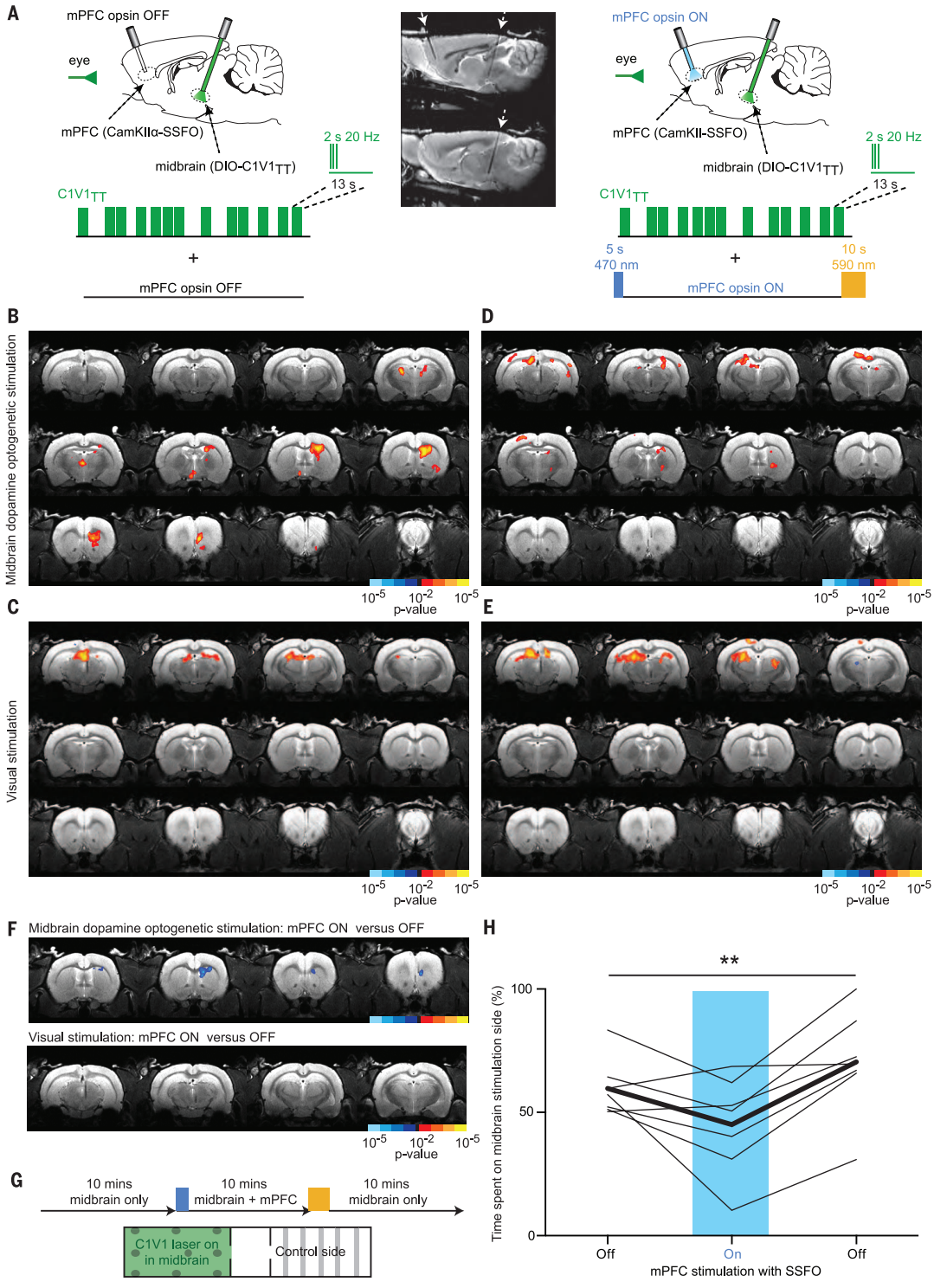

Fig. 5. Cortical suppression of striatal BOLD and behavioral response to midbrain dopaminergic stimulation. (**A**) Schematic illustrating the design of the dual-stimulation experiment. The sagittal T2 anatomy scan (two adjacent sections shown) demonstrates the angled orientation of the two fibers. (**B**) Brain-wide *Z*-score map of BOLD activity in response to C1V1$_{TT}$ stimulation in midbrain dopaminergic neurons and (**C**) visual stimulation alone (n = 6 rats, 32 runs). (**D**) *Z*-score map in response to C1V1$_{TT}$ stimulation and (**E**) visual stimulation in combination with SSFO activation in the mPFC (n = 6 rats, 32 runs). (**F**) Statistical comparison of mPFC-activated versus nonactivated condition for midbrain dopaminergic stimulation and visual stimulation. (**G**) Real-time place preference test for C1V1$_{TT}$ stimulation alone and in combination with mPFC activation with SSFO. The percentage of time spent on the C1V1$_{TT}$ stimulation side was assessed for all three bursts. (**H**) One-way repeated measures ANOVA shows a significant effect of mPFC activation (**P = 0.0047, F = 8.652, number of groups = 3, number of rats = 7), with a significant difference from baseline and washout conditions after Newman-Keuls multiple comparison testing.

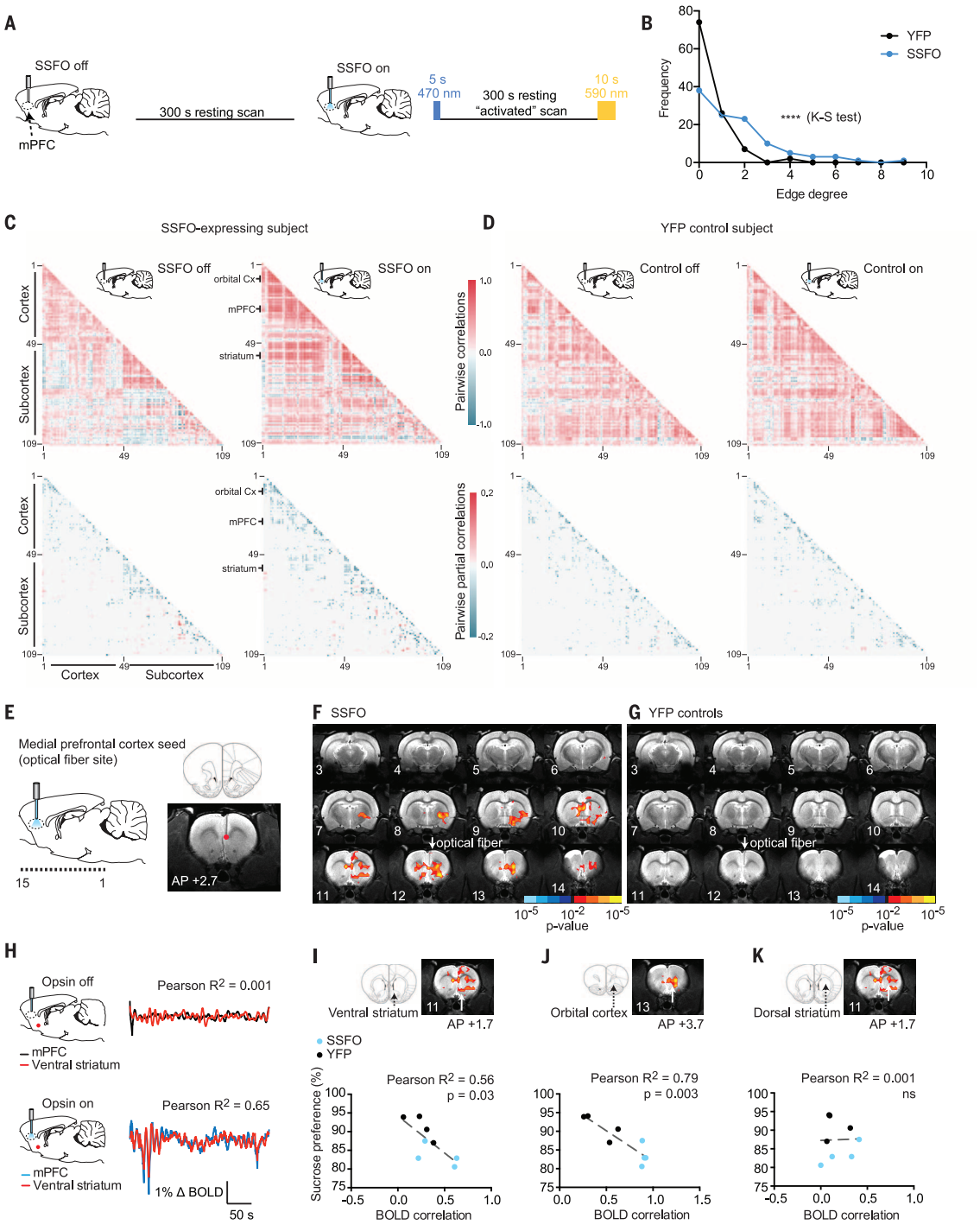

Fig. 6. Evoked changes in brainwide interregional relationships and joint statistics after focal optogenetic modulation of mPFC excitability. (**A**) Brainwide graphical analysis was performed on resting-state fMRI scans for SSFO-expressing and YFP-control subjects to assess changes in BOLD activity partial correlations between mPFC-activated versus nonactivated scans. (**B**) Change in edge degree distribution across SSFO (n = 4 rats, 14 runs) and YFP subjects (n = 4 rats, 15 runs) in response to mPFC activation by light (Kolmogov-Smirnov test for difference in distributions between SSFO and YFP groups: D = 0.3394, ****P < 0.0001). (**C**) Pairwise correlation and sparse partial correlation matrices for 109 brain regions for an example SSFO-expressing subject and (**D**) a YFP-control subject under nonactivated and mPFC-activated conditions. Each matrix represents the data from a single scan. Brain regions (individual ROIs) are labeled by number; the index key is provided in fig. S12. Selected brain regions have been highlighted. (**E**) Seed-based correlation analysis (for mPFC seed). (**F**) Z-score map for changes in correlated BOLD activity with mPFC after SSFO activation for SSFO-expressing subjects (n = 4 rats, 14 runs) and (**G**) YFP-control subjects (n = 4 rats, 15 runs). (**H**) Example BOLD activity time series in two ROIs: mPFC (black or blue) and ventral striatum (red) during opsin-off (Pearson R^2 = 0.001, P = 0.06) and opsin-on (Pearson R^2 = 0.65, P < 0.0001) conditions. (**I** to **K**) Relationship between sucrose preference and mPFC-activated BOLD correlations between the mPFC and three brain regions for SSFO-expressing (blue, n = 4 rats) and YFP-control subjects (black, n = 4 rats). (I) Ventral striatum (Pearson R^2 = 0.56, P = 0.032, n = 8 pairs). (J) Orbital cortex (Pearson R^2 = 0.79, P = 0.0031, n = 8 pairs). (K) Dorsal striatum (Pearson R^2 = 0.001, P = 0.95, n = 8 pairs).

Elevated mPFC excitability suppresses striatal responses to dopamine

We next sought to determine whether this altered behavior might be associated with disrupted recruitment of the striatal response to activation of midbrain dopamine neurons. We performed a dual–optogenetic stimulation experiment in which we expressed a red-shifted channelrhodopsin variant ($C1V1_{TT}$) via a Cre-dependent construct within the midbrain dopamine neurons of TH-Cre transgenic rats, as well as the blue light–activated SSFO in the mPFC under the CaMKIIα promoter in the same rats (Fig. 5A). In the MRI scanner, we used an event-related design (560 nm, 2 s of 20-Hz light pulses, 10-ms pulse width) to stimulate $C1V1_{TT}$, with visual stimulation in parallel as described above. In interleaved, matched scans, we superimposed mPFC activation with SSFO, using a 5-s pulse of blue light (470 nm) to the mPFC before the start of the scan and a 10-s pulse of yellow light (590 nm) to inactivate SSFO at the end of the scan. Although visual responses were similar between the two types of scans (Fig. 5, C, E, and F), we observed significant suppression of the evoked striatal BOLD response to $C1V1_{TT}$-mediated dopaminergic stimulation when the mPFC was activated, compared with when the mPFC was not activated (Fig. 5, B, D, and F; and table S6).

We performed a real-time place preference test in which rats were free to explore two chambers for a total of 30 min, during which time $C1V1_{TT}$ stimulation of dopaminergic cells was continually paired with one chamber. The test began with a 10-min period in which SSFO was not active, then followed by 10 min of superimposed mPFC activation by SSFO (single 5-s pulse of blue light in mPFC at the start, 10-s pulse of yellow light at the end), and finally followed by a final 10 min with SSFO inactive again (Fig. 5G). At baseline, rats tended to preferentially seek out the chamber in which they received midbrain dopamine neuron stimulation, but in the presence of superimposed mPFC activation by SSFO, no such preference was exhibited. Once SSFO was switched off, the sensitivity to midbrain dopamine neuron stimulation returned, as indicated by increased time spent in the $C1V1_{TT}$ stimulation chamber (Fig. 5H).

Elevated mPFC excitability triggers spatiotemporally correlated BOLD activity among distant brain regions and predicts anhedonic behavior

Altered resting-state correlations between the prefrontal cortex and a network of brain regions have been observed in neuroimaging studies of patients with depression (*43*), schizophrenia, and other psychiatric conditions (*24*) for which anhedonia is a prominent symptom. However, causal circuit mechanisms by which these relationships could be altered remain unknown. We hypothesized that stably increasing mPFC excitability would causally modulate resting-state spatiotemporal activity relationships between distant brain structures. We performed resting-state fMRI scans in which rats were either scanned with no optogenetic stimulation at all (nonactivated) or scanned in the mPFC-activated state, in which a 5-s blue light pulse was delivered to activate SSFO before initiation of a 5-min scan. After completion of the activated scan, a 10-s yellow light pulse was delivered to deactivate SSFO (Fig. 6A). No visual stimulation was delivered during these experiments, and nonactivated and activated scans were interleaved over the course of the scanning sessions.

Increased excitability of mPFC CaMKIIα-expressing neurons in awake rats modulated spontaneous BOLD activity fluctuations and resting-state relationships among a number of distinct cortical and subcortical brain regions. To explore these brainwide changes in an unbiased manner, we segmented the brain into 109 anatomical regions defined a priori (fig. S11A), extracted the time course of spontaneous activity during each scan for each brain region, and estimated sparse partial correlations with graphical lasso (*52*, *53*) to identify brain regions (or nodes) with significant changes in connection strength (edge degree) after mPFC activation (Fig. 6, B to D, and fig. S11, B to F). In SSFO-expressing subjects, we found a greater change in the number of significant partial correlations (hereafter referred to as "connection changes") between activated versus nonactivated scans, compared with the YFP-control group (Fig. 6B and figs. S11, C to F, and S12). Many regions—such as the mPFC with the orbital cortex and ventral striatum (Fig. 6C) and the cingulate cortex with the dorsal striatum—became more strongly interconnected after mPFC SSFO activation. The lateral orbital cortex, although not a direct target of the optogenetic excitability change, exhibited the greatest number of connection changes, linking with other areas of the frontal cortex, as well as subcortical regions such as the ventral striatum, claustrum, and septum. Relatively fewer regions became more isolated; these included the auditory and retrosplenial cortices, regions that have been clinically implicated in both depression and schizophrenia (*54*, *55*). Far fewer changes were detected in YFP controls, and these predominantly included lost connections, which could partially reflect alterations in spontaneous BOLD activity due to local metabolic or temperature changes (*26*) or simply temporal drift (figs. S11B and S12).

We next turned to a traditional seed-based analysis (Fig. 6E). Using the time course of spontaneous BOLD activity from a seed at the tip of the optical fiber in mPFC, we confirmed that a number of brain regions—including the orbital cortex, the dorsal and ventral striatum, and the septum—showed significantly increased correlation with fiber site activity after mPFC activation with SSFO (Fig. 6, F and H). No significant changes were observed for YFP-control subjects (Fig. 6G), and the between-group difference (SSFO versus YFP) in correlated activity was significant (fig. S9C and table S7). We considered whether such resting-state BOLD activity correlations could predict the behavioral changes elicited by mPFC activation, in subjects that had participated in behavioral testing as well as fMRI scanning. The strength of BOLD activity correlation between the mPFC and ventral striatum and orbital cortex during SSFO stimulation predicted the degree of anhedonic behavior. This was not true of the dorsal striatum, implying that circuit-specific changes in functional connections can predict behavioral phenotype (Fig. 6, I to K). Moreover, in contrast to these long-range interactions between brain regions, local evoked increases in BOLD activity in the mPFC alone were not sufficient to account for the emergence of the anhedonic behavioral phenotype (fig. S10A), demonstrating the importance of this brainwide analysis.

To explore SSFO-mediated changes in neural signals on a finer time scale, we used dual-site in vivo electrophysiological recordings in the mPFC and the striatum, simultaneously recording local field potentials (LFPs) at each site before and after shifts in mPFC excitability (fig. S13). Coherence in the LFP (in particular, the gamma frequency band, >30 Hz) has been suggested to play a role in mediating functional connectivity across anatomically distributed brain regions (*56*–*59*). Because we have found that elevation in mPFC activity causes increased high-frequency gamma power in the mPFC (*23*) and increased correlated activity between the mPFC and the striatum on longer time scales (Fig. 6), we hypothesized that increased coherence in the gamma frequency range between the mPFC and the striatum might appear after focal elevations in mPFC excitability. Multielectrode arrays were implanted into the mPFC (in addition to an optical fiber) and the striatum (fig. S13A). We recorded the LFP in these two regions at baseline (before light delivery) and after a 2-s pulse of blue light (fig. S13B). After SSFO activation, we observed a reduction in LFP power in the slow gamma frequency range (30 to 40 Hz), with a relative preservation (in the mPFC) or increase (in the striatum) in the fast gamma range (70 to 80 Hz) range (fig. S13, C and D). Across all subjects, this resulted in a significant increase in the ratio of fast to slow gamma power in the striatum (fig. S13E), as well as an increase in LFP coherence between the mPFC and the striatum across the gamma (and even high beta) range of frequencies (fig. S13, F and G). Single-unit recordings of neural spiking in the striatum simultaneous with SSFO activation in the mPFC demonstrated that striatal units showed a mixed pattern of spiking activity in the 500-ms period after a pulse of blue light, with 44% of units exhibiting an increase in spiking and 42% showing a decrease, compared with spiking activity during the 500-ms period preceding the light pulse (fig. S8, F to I). LFP synchrony between brain regions thus represents a complex phenomenon involving both excitatory and inhibitory interactions at the single-cell level (*60*).

Discussion

We have combined focal, cell-type–specific chronic and acute optogenetic manipulations together with fMRI, behavioral testing, and in vivo

electrophysiological recordings to probe interactions between cortical and subcortical brain regions causally involved in reward-related behavior. The major advances of this study are threefold. First, we demonstrate that stimulation of midbrain dopamine neurons is sufficient to increase BOLD activity in the striatum, in a manner correlated with reward-seeking behavior across individual subjects, addressing a long-standing controversy over the potential source of reward-related striatal BOLD activity in human fMRI studies. Second, elevated excitability of the mPFC was found to reduce both striatal BOLD responses to the stimulation of dopamine neurons and the behavioral drive to seek stimulation of dopamine neurons. Thus, the mPFC exerts top-down control over the interaction between the dopaminergic midbrain and the striatum to modulate the expression of reward-related behavior. Finally, stably elevating the excitability of mPFC pyramidal neurons was sufficient to drive changes in corticolimbic BOLD synchrony, as well as corresponding anhedonic behavior, resembling imaging and clinical phenotypes observed in human psychiatric disease. These findings suggest that, rather than acting in parallel, dopaminergic and top-down cortical projections are instead intersecting at the striatum and working in concert to regulate reward processing, with implications for our understanding of the pathogenesis of anhedonia.

The striatum receives midbrain dopaminergic and cortical glutamatergic inputs (*8*, *61*, *62*) and is therefore ideally positioned to both motivate and modulate reward-related behavior (*3*, *42*, *63*). We first observed that specific optogenetic drive of midbrain dopaminergic neurons increased striatal BOLD activity and that rats with greater ventral striatal BOLD activity in the scanner worked harder for optogenetic stimulation of midbrain dopamine neurons in the operant chamber. The observed increases in ventral striatal BOLD activity could be blunted by administration of dopaminergic antagonists and exhibited a similar temporal profile to BOLD activity measured during reward anticipation in humans (*64*). Optogenetic inhibition, on the other hand, reduced BOLD activity in the dorsal striatum, as well as in other unexpected brain regions, such as the hypothalamus, suggesting that the spatial influence of changes in tonic dopamine may differ from that of phasic dopamine. These results alone bridge a gap in our current understanding of dopamine signaling. Previously, researchers have used fast-scan cyclic voltammetry to track dopamine release in selected projection regions (*30*, *65*, *66*) and electrophysiology readouts to investigate the firing of downstream neurons in response to dopamine release (*32*, *51*, *67*). Meanwhile, neuroimaging studies in humans and animals have identified mesolimbic BOLD activity in response to reward-related cues and outcomes (*68*–*71*). However, no causal link had yet been established between defined firing of midbrain dopamine neurons and BOLD activity, but making this connection is crucial for interpretation of BOLD studies in reward-related behavior. Although one might predict that dopamine neuron activation could increase BOLD activity in terminal projection regions, such an association cannot be assumed, because activation of postsynaptic dopamine receptors has diverse modulatory influences through intracellular G protein cascades.

Although we found that reward-seeking behavior increased monotonically with stimulation duration (up to and beyond 2 s), and stimulation of dopamine neurons for 2 s (at 20 Hz, 10-ms pulse width) was more effective than shorter burst durations for eliciting striatal BOLD, in future work it will be interesting to compare further burst and tonic stimulation frequencies in different experimental contexts, which may drive different physiological states and BOLD responses with important consequences for behavior. Additionally, dopamine receptor blockade increased BOLD activity in response to visual stimulation, suggesting that dopamine might modulate aspects of primary sensory processing; this finding prompts many questions about how other neuromodulators (such as serotonin, acetylcholine, and noradrenaline) influence BOLD activity in health or disease. Another area for exploration is the role of co-released neurotransmitters. For example, glutamate exhibits stronger co-release in the ventral compared with the dorsal striatum (*72*). Our pharmacological data show that ventral striatal BOLD was completely suppressed by dopaminergic antagonists, supporting the hypothesis that this signal results from dopamine release. However, analysis of our fiber tip placement in the midbrain (located within the medial-lateral and anterior-posterior spatial extent of the VTA in all animals) suggests that lateral rather than medial VTA fiber placement most effectively increased BOLD activity in the ventral and dorsal striatum (although placement did not significantly influence behavioral responding) (fig. S4). This finding is consistent with recent work showing that the medial VTA projects most strongly to the medial nucleus accumbens (*73*), mapping spatially to sites of vesicular glutamate transporter 2 (VGLUT2)–associated glutamate co-release (*72*), whereas the lateral VTA projects more broadly to the lateral nucleus accumbens and dorsal striatum (*73*). Experiments that establish the role of neurotransmitter co-release in BOLD activity might involve the use of conditional VGLUT2 knockout in dopamine neurons.

Next, we turned to pathophysiological processes that may blunt reward-seeking behavior and contribute to the clinical symptom of anhedonia. Neuroimaging studies in human patients with depression have identified a region of the mPFC (subgenual cingulate gyrus) that exhibits elevated activity (*11*) in correlation with severity of anhedonic symptoms (*15*). The subgenual cingulate becomes increasingly connected within resting-state brain networks in depressed patients, and this network effect is associated with disease refractoriness (*43*). Treatment of depression with the mixed-effect glutamate receptor antagonist ketamine may also improve anhedonic symptoms and increase striatal metabolism (*74*). Imaging studies in patients with schizophrenia have similarly pointed to altered patterns of neural activity associated with anhedonia (*16*, *75*, *76*). These studies led us to hypothesize that dysregulation of long-range neuronal interactions triggered by elevated mPFC excitability could contribute to anhedonia in neuropsychiatric disease (*7*, *8*, *77*). Enhanced mPFC excitability in rats led to specific synchronization of physiological signals (both BOLD and LFP) between the mPFC and connected subcortical regions, and the degree of synchrony between specific brain regions (mPFC, orbital cortex, ventral striatum) correlated with the expression of anhedonic behavior in individual animals. Modulating the excitability of specific cell populations is thus sufficient to drive changes in BOLD activity correlations between brain regions, resembling those observed in human psychiatric disorders. The downstream effect of this phenomenon became most apparent in the context of concurrent dopaminergic stimulation, when mPFC hyperexcitability exerted a top-down suppressive effect on reward-related neural signaling in the striatum and reward-seeking behavior.

The clinical background guiding our work was increased mPFC excitability and fMRI BOLD activity, rather than a specific spiking pattern in a particular cell type. We chose to use SSFO, which does not act via coordinated activation of expressing neurons at a firing frequency chosen by the experimenter, but instead elicits an asynchronous enhancement in excitability by causing subthreshold depolarization (*23*, *25*). Crucially, this manipulation exerted its downstream effects on functional connectivity rather than on the univariate BOLD signal locally or in predicted projection areas. Moreover, this distinct BOLD effect was correlated with a decrease rather than an increase in hedonic behavior. This approach had the additional practical advantages of permitting BOLD signal acquisition without continuous light delivery in the scanner (avoiding the potential for tissue heating) and facilitating chronic manipulations of excitability over days in the appetitive behavioral assays.

Low-frequency electrical stimulation (10 Hz; typical of mPFC neural activity during cognitive tasks) can reduce dopamine release in the striatum, whereas high-frequency electrical stimulation at 60 to 200 Hz can have the opposite effect (*78*). These contrasting observations may relate to the finding that high-frequency (and possibly supraphysiological at ~100 Hz) burst stimulation of the mPFC can exert antidepressant effects in mice (*48*, *79*) and humans (*11*). When mPFC firing rates were mildly and asynchronously elevated within a physiological range by SSFO (fig. S8B), we observed blunting of the striatal response to dopaminergic input and anhedonic effects on behavior. The precise circuit mechanisms of the prefrontal influence on these subcortical interactions could occur via feed-forward inhibition in the striatum, the midbrain, or another intermediary brain region. Alternatively, mPFC activity could increase tonic dopamine release in the striatum, producing a ceiling effect on further dopaminergic signaling and potentially thereby

preventing bursts of dopamine stimulation from evoking phasic BOLD activity in the striatum, as well as diminishing reward-related behavior. As noted in earlier work, in the context of modulation of phasic BOLD activity by dopaminergic drugs (i.e., amphetamine) in humans (*64*), task (or stimulation)–based fMRI cannot readily distinguish a reduction in evoked BOLD activity from a ceiling effect. However, a lack of locomotor stimulation during combined mPFC and dopaminergic stimulation (fig. S14) suggests reduced rather than increased tonic dopamine levels (*80*).

Our large data set (http://clarityresourcecenter.org/ofMRI.html) forms a resource for understanding and modeling dynamic brainwide activity patterns that are causally linked to adaptive and maladaptive reward states. Our ofMRI findings constitute a bridge between the worlds of animal optogenetics and clinical neuroimaging and provide causal evidence for behaviorally meaningful competition between two brain regions for influence over a third region (in this case, between dopaminergic midbrain and glutamatergic prefrontal cortex neurons for influence over the striatum). In a healthy brain, descending projections from the cortex to subcortical limbic regions may be important for guiding behavioral responses to rewarding or salient stimuli (*81*), whereas in clinical anhedonia, increased mPFC excitability may generate a hypersynchronous state between specific cortical (mPFC, orbital cortex) and subcortical (ventral striatum) brain regions, which in turn suppresses the response to neuromodulatory (dopaminergic) signals normally important for reward.

Methods summary

See the supplementary materials for full details of the materials and methods (*82*). A number of key technical refinements allowed us to more readily visualize BOLD responses to a variety of stimuli. First, to scan awake rodents, we constructed a customized MRI-compatible head-fixation apparatus and habituated rats to the scanner environment to minimize stress and motion (as described above). Second, we optimized functional data acquisition using fast single-shot (0.5-s TR; spiral-in/out) image acquisition protocols (*83*–*85*), which minimized motion artifacts from image fusion and reduced susceptibility artifacts from implanted material or airspaces in the skull. Functional images encompassed the cerebral hemispheres (but not the cerebellum), with signal maintained in most brain regions. However, some dropout occurred in posterior ventrolateral regions, including portions of the temporal association cortices, entorhinal cortices, and posteroventral parts of the hippocampus (fig. S1B). Third, we used a pseudorandomly ordered event-related stimulus sequence, which maximized the number of trials per scan while still affording resolution of phasic responses to optogenetic stimulation. Specifically, the maximum length sequence (m-sequence) design (*86*) allowed simultaneous but noncorrelated presentation of two stimuli, such that optogenetic stimulation occurred while a positive-control stimulus (i.e., a visual stimulus) was also applied, to allow verification of BOLD responses to sensory input in experiments in which the BOLD response to optogenetic stimulation might be absent or reduced (e.g., YFP controls, pharmacological manipulations, or dual-stimulation optogenetic experiments). During pilot testing, we noticed that the hemodynamic response function (HRF) to SSFO and visual stimulation differed from that observed in response to ChR2 stimulation of dopamine neurons and from the HRF commonly observed in humans (*87*). We found that for SSFO and visual stimulation, the HRF more closely followed a customized model, with exponential rise and decay (τ = 7 s) (fig. S15). Although modeling with the canonical human HRF replicated our results, the rat-specific model more effectively resolved activity in SSFO and visual experiments. Although the hemodynamic responses of different species might vary for a number of reasons (e.g., differences in the properties of rat capillary networks), they may also vary as a function of brain region (e.g., cortical versus subcortical), neurotransmitter release (dopamine versus glutamate), or the eliciting method of stimulation (e.g., ChR2 versus SSFO). Based on these findings, we recommend that investigators closely inspect raw data acquired in ofMRI experiments before applying models optimized for human data, to ensure that divergent temporal features of the rat HRF are considered.

REFERENCES AND NOTES

1. A. E. Kelley, K. C. Berridge, The neuroscience of natural rewards: Relevance to addictive drugs. *J. Neurosci.* **22**, 3306–3311 (2002). pmid: 11978804
2. W. Schultz, Predictive reward signal of dopamine neurons. *J. Neurophysiol.* **80**, 1–27 (1998). pmid: 9658025
3. S. R. Sesack, A. A. Grace, Cortico-basal ganglia reward network: Microcircuitry. *Neuropsychopharmacology* **35**, 27–47 (2010). doi: 10.1038/npp.2009.93; pmid: 19675534
4. M. W. Howe, P. L. Tierney, S. G. Sandberg, P. E. M. Phillips, A. M. Graybiel, Prolonged dopamine signalling in striatum signals proximity and value of distant rewards. *Nature* **500**, 575–579 (2013). doi: 10.1038/nature12475; pmid: 23913271
5. C. D. Fiorillo, P. N. Tobler, W. Schultz, Discrete coding of reward probability and uncertainty by dopamine neurons. *Science* **299**, 1898–1902 (2003). doi: 10.1126/science.1077349; pmid: 12649484
6. P. Gorwood, Neurobiological mechanisms of anhedonia. *Dialogues Clin. Neurosci.* **10**, 291–299 (2008). pmid: 18979942
7. E. J. Nestler, W. A. Carlezon Jr., The mesolimbic dopamine reward circuit in depression. *Biol. Psychiatry* **59**, 1151–1159 (2006). doi: 10.1016/j.biopsych.2005.09.018; pmid: 16566899
8. S. J. Russo, E. J. Nestler, The brain reward circuitry in mood disorders. *Nat. Rev. Neurosci.* **14**, 609–625 (2013). doi: 10.1038/nrn3381; pmid: 23942470
9. K. Deisseroth, Circuit dynamics of adaptive and maladaptive behaviour. *Nature* **505**, 309–317 (2014). doi: 10.1038/nature12982; pmid: 24429629
10. B. Moghaddam, J. Wood, Teamwork matters: Coordinated neuronal activity in brain systems relevant to psychiatric disorders. *JAMA Psychiatry* **71**, 197–199 (2014). doi: 10.1001/jamapsychiatry.2013.2080; pmid: 24305975
11. H. S. Mayberg *et al*., Deep brain stimulation for treatment-resistant depression. *Neuron* **45**, 651–660 (2005). doi: 10.1016/j.neuron.2005.02.014; pmid: 15748841
12. R. T. Dunn *et al*., Principal components of the Beck Depression Inventory and regional cerebral metabolism in unipolar and bipolar depression. *Biol. Psychiatry* **51**, 387–399 (2002). doi: 10.1016/S0006-3223(01)01244-6; pmid: 11904133
13. M. T. Mitterschiffthaler *et al*., Neural response to pleasant stimuli in anhedonia: An fMRI study. *Neuroreport* **14**, 177–182 (2003). doi: 10.1097/00001756-200302100-00003; pmid: 12598724
14. V. Kumari *et al*., Neural abnormalities during cognitive generation of affect in treatment-resistant depression. *Biol. Psychiatry* **54**, 777–791 (2003). doi: 10.1016/S0006-3223(02)01785-7; pmid: 14550677
15. P. A. Keedwell, C. Andrew, S. C. R. Williams, M. J. Brammer, M. L. Phillips, The neural correlates of anhedonia in major depressive disorder. *Biol. Psychiatry* **58**, 843–853 (2005). doi: 10.1016/j.biopsych.2005.05.019; pmid: 16043128
16. P.-O. Harvey, J. Pruessner, Y. Czechowska, M. Lepage, Individual differences in trait anhedonia: A structural and functional magnetic resonance imaging study in non-clinical subjects. *Mol. Psychiatry* **12**, 767–775 (2007).doi: 10.1038/sj.mp.4002045; pmid: 17505465
17. K. J. Ressler, H. S. Mayberg, Targeting abnormal neural circuits in mood and anxiety disorders: From the laboratory to the clinic. *Nat. Neurosci.* **10**, 1116–1124 (2007). doi: 10.1038/nn1944; pmid: 17726478
18. M. T. Berlim, A. McGirr, F. Van den Eynde, M. P. A. Fleck, P. Giacobbe, Effectiveness and acceptability of deep brain stimulation (DBS) of the subgenual cingulate cortex for treatment-resistant depression: A systematic review and exploratory meta-analysis. *J. Affect. Disord.* **159**, 31–38 (2014). doi: 10.1016/j.jad.2014.02.016; pmid: 24679386
19. J. P. O'Doherty, Reward representations and reward-related learning in the human brain: Insights from neuroimaging. *Curr. Opin. Neurobiol.* **14**, 769–776 (2004). doi: 10.1016/j.conb.2004.10.016; pmid: 15582382
20. B. Knutson, J. C. Cooper, Functional magnetic resonance imaging of reward prediction. *Curr. Opin. Neurol.* **18**, 411–417 (2005). doi: 10.1097/01.wco.0000173463.24758.f6; pmid: 16003117
21. E. S. Boyden, F. Zhang, E. Bamberg, G. Nagel, K. Deisseroth, Millisecond-timescale, genetically targeted optical control of neural activity. *Nat. Neurosci.* **8**, 1263–1268 (2005). doi: 10.1038/nn1525; pmid: 16116447
22. V. Gradinaru, K. R. Thompson, K. Deisseroth, eNpHR: A *Natronomonas* halorhodopsin enhanced for optogenetic applications. *Brain Cell Biol.* **36**, 129–139 (2008). doi: 10.1007/s11068-008-9027-6; pmid: 18677566
23. O. Yizhar *et al*., Neocortical excitation/inhibition balance in information processing and social dysfunction. *Nature* **477**, 171–178 (2011). doi: 10.1038/nature10360; pmid: 21796121
24. N. D. Woodward, C. J. Cascio, Resting-state functional connectivity in psychiatric disorders. *JAMA Psychiatry* **72**, 743–744 (2015). doi: 10.1001/jamapsychiatry.2015.0484; pmid: 26061674
25. A. Berndt, O. Yizhar, L. A. Gunaydin, P. Hegemann, K. Deisseroth, Bi-stable neural state switches. *Nat. Neurosci.* **12**, 229–234 (2009). doi: 10.1038/nn.2247; pmid: 19079251
26. I. N. Christie *et al*., fMRI response to blue light delivery in the naïve brain: Implications for combined optogenetic fMRI studies. *Neuroimage* **66**, 634–641 (2013). doi: 10.1016/j.neuroimage.2012.10.074; pmid: 23128081
27. F. Zhang *et al*., Red-shifted optogenetic excitation: A tool for fast neural control derived from *Volvox carteri*. *Nat. Neurosci.* **11**, 631–633 (2008). doi: 10.1038/nn.2120; pmid: 18432196
28. M. A. Pisauro, N. T. Dhruv, M. Carandini, A. Benucci, Fast hemodynamic responses in the visual cortex of the awake mouse. *J. Neurosci.* **33**, 18343–18351 (2013). doi: 10.1523/JNEUROSCI.2130-13.2013; pmid: 24227743
29. H.-C. Tsai *et al*., Phasic firing in dopaminergic neurons is sufficient for behavioral conditioning. *Science* **324**, 1080–1084 (2009). doi: 10.1126/science.1168878; pmid: 19389999
30. I. B. Witten *et al*., Recombinase-driver rat lines: Tools, techniques, and optogenetic application to dopamine-mediated reinforcement. *Neuron* **72**, 721–733 (2011). doi: 10.1016/j.neuron.2011.10.028; pmid: 22153370
31. N. K. Logothetis, J. Pauls, M. Augath, T. Trinath, A. Oeltermann, Neurophysiological investigation of the basis of the fMRI signal. *Nature* **412**, 150–157 (2001). doi: 10.1038/35084005; pmid: 11449264
32. K. M. Tye *et al*., Dopamine neurons modulate neural encoding and expression of depression-related behaviour. *Nature* **493**, 537–541 (2013). doi: 10.1038/nature11740; pmid: 23235822
33. G. H. Glover, S. K. Lemieux, M. Drangova, J. M. Pauly, Decomposition of inflow and blood oxygen level-dependent (BOLD) effects with dual-echo spiral gradient-recalled echo (GRE) fMRI. *Magn. Reson. Med.* **35**, 299–308 (1996). doi: 10.1002/mrm.1910350306; pmid: 8699940
34. J. A. Bourne, SCH 23390: The first selective dopamine D_1-like receptor antagonist. *CNS Drug Rev.* **7**, 399–414 (2001). doi: 10.1111/j.1527-3458.2001.tb00207.x; pmid: 11830757

35. S. P. S *et al*., A highly sensitive LC-MS/MS method for the determination of *S*-raclopride in rat plasma: Application to a pharmacokinetic study in rats. *Biomed. Chromatogr.* **25**, 930–937 (2011). doi: 10.1002/bmc.1547; pmid: 21154642
36. B. Noudoost, T. Moore, Control of visual cortical signals by prefrontal dopamine. *Nature* **474**, 372–375 (2011). doi: 10.1038/nature09995; pmid: 21572439
37. J. T. Arsenault, K. Nelissen, B. Jarraya, W. Vanduffel, Dopaminergic reward signals selectively decrease fMRI activity in primate visual cortex. *Neuron* **77**, 1174–1186 (2013). doi: 10.1016/j.neuron.2013.01.008; pmid: 23522051
38. D. Zaldivar, A. Rauch, K. Whittingstall, N. K. Logothetis, J. Goense, Dopamine-induced dissociation of BOLD and neural activity in macaque visual cortex. *Curr. Biol.* **24**, 2805–2811 (2014). doi: 10.1016/j.cub.2014.10.006; pmid: 25456449
39. F. De Martino *et al*., Combining multivariate voxel selection and support vector machines for mapping and classification of fMRI spatial patterns. *Neuroimage* **43**, 44–58 (2008). doi: 10.1016/j.neuroimage.2008.06.037; pmid: 18672070
40. A. A. Grace, Phasic versus tonic dopamine release and the modulation of dopamine system responsivity: A hypothesis for the etiology of schizophrenia. *Neuroscience* **41**, 1–24 (1991). doi: 10.1016/0306-4522(91)90196-U; pmid: 1676137
41. P. N. Tobler, A. Dickinson, W. Schultz, Coding of predicted reward omission by dopamine neurons in a conditioned inhibition paradigm. *J. Neurosci.* **23**, 10402–10410 (2003). pmid: 14614099
42. A. Ghazizadeh, F. Ambroggi, N. Odean, H. L. Fields, Prefrontal cortex mediates extinction of responding by two distinct neural mechanisms in accumbens shell. *J. Neurosci.* **32**, 726–737 (2012). doi: 10.1523/JNEUROSCI.3891-11.2012; pmid: 22238108
43. M. D. Greicius *et al*., Resting-state functional connectivity in major depression: Abnormally increased contributions from subgenual cingulate cortex and thalamus. *Biol. Psychiatry* **62**, 429–437 (2007). doi: 10.1016/j.biopsych.2006.09.020; pmid: 17210143
44. J. D. Berke, Functional properties of striatal fast-spiking interneurons. *Front. Syst. Neurosci.* **5**, 45 (2011). doi: 10.3389/fnsys.2011.00045; pmid: 21743805
45. J. H. Lee *et al*., Global and local fMRI signals driven by neurons defined optogenetically by type and wiring. *Nature* **465**, 788–792 (2010). doi: 10.1038/nature09108; pmid: 20473285
46. A. M. Aravanis *et al*., An optical neural interface: In vivo control of rodent motor cortex with integrated fiberoptic and optogenetic technology. *J. Neural Eng.* **4**, S143–S156 (2007). doi: 10.1088/1741-2560/4/3/S02; pmid: 17873414
47. H. W. Berendse, Y. Galis-de Graaf, H. J. Groenewegen, Topographical organization and relationship with ventral striatal compartments of prefrontal corticostriatal projections in the rat. *J. Comp. Neurol.* **316**, 314–347 (1992). doi: 10.1002/cne.903160305; pmid: 1577988
48. C. Hamani *et al*., Antidepressant-like effects of medial prefrontal cortex deep brain stimulation in rats. *Biol. Psychiatry* **67**, 117–124 (2010). doi: 10.1016/j.biopsych.2009.08.025; pmid: 19819426
49. D. Chaudhury *et al*., Rapid regulation of depression-related behaviours by control of midbrain dopamine neurons. *Nature* **493**, 532–536 (2013). doi: 10.1038/nature11713; pmid: 23235832
50. B. K. Lim, K. W. Huang, B. A. Grueter, P. E. Rothwell, R. C. Malenka, Anhedonia requires MC4R-mediated synaptic adaptations in nucleus accumbens. *Nature* **487**, 183–189 (2012). doi: 10.1038/nature11160; pmid: 22785313
51. L. A. Gunaydin *et al*., Natural neural projection dynamics underlying social behavior. *Cell* **157**, 1535–1551 (2014). doi: 10.1016/j.cell.2014.05.017; pmid: 24949967
52. J. Friedman, T. Hastie, R. Tibshirani, Sparse inverse covariance estimation with the graphical lasso. *Biostatistics* **9**, 432–441 (2008). doi: 10.1093/biostatistics/kxm045; pmid: 18079126
53. T. Zhao, H. Liu, K. Roeder, J. Lafferty, L. Wasserman, The huge package for high-dimensional undirected graph estimation in R. *J. Mach. Learn. Res.* **13**, 1059–1062 (2012).
54. R. L. Bluhm *et al*., Retrosplenial cortex connectivity in schizophrenia. *Psychiatry Res. Neuroimaging* **174**, 17–23 (2009). doi: 10.1016/j.pscychresns.2009.03.010; pmid: 19783410
55. M. de la Iglesia-Vaya *et al*., Abnormal synchrony and effective connectivity in patients with schizophrenia and auditory hallucinations. *NeuroImage Clin.* **6**, 171–179 (2014). doi: 10.1016/j.nicl.2014.08.027; pmid: 25379429
56. G. G. Gregoriou, S. J. Gotts, H. Zhou, R. Desimone, High-frequency, long-range coupling between prefrontal and visual cortex during attention. *Science* **324**, 1207–1210 (2009). doi: 10.1126/science.1171402; pmid: 19478185
57. M. Siegel, T. H. Donner, A. K. Engel, Spectral fingerprints of large-scale neuronal interactions. *Nat. Rev. Neurosci.* **13**, 121–134 (2012). pmid: 22233726
58. K. M. Igarashi, L. Lu, L. L. Colgin, M.-B. Moser, E. I. Moser, Coordination of entorhinal-hippocampal ensemble activity during associative learning. *Nature* **510**, 143–147 (2014). doi: 10.1038/nature13162; pmid: 24739966
59. G. Buzsáki, X.-J. Wang, Mechanisms of gamma oscillations. *Annu. Rev. Neurosci.* **35**, 203–225 (2012). doi: 10.1146/annurev-neuro-062111-150444; pmid: 22443509
60. G. Buzsáki, C. A. Anastassiou, C. Koch, The origin of extracellular fields and currents—EEG, ECoG, LFP and spikes. *Nat. Rev. Neurosci.* **13**, 407–420 (2012). doi: 10.1038/nrn3241; pmid: 22595786
61. S. Ikemoto, Dopamine reward circuitry: Two projection systems from the ventral midbrain to the nucleus accumbens-olfactory tubercle complex. *Brain Res. Rev.* **56**, 27–78 (2007). doi: 10.1016/j.brainresrev.2007.05.004; pmid: 17574681
62. S. N. Haber, B. Knutson, The reward circuit: Linking primate anatomy and human imaging. *Neuropsychopharmacology* **35**, 4–26 (2010). doi: 10.1038/npp.2009.129; pmid: 19812543
63. T. W. Robbins, B. J. Everitt, Neurobehavioural mechanisms of reward and motivation. *Curr. Opin. Neurobiol.* **6**, 228–236 (1996). doi: 10.1016/S0959-4388(96)80077-8; pmid: 8725965
64. B. Knutson *et al*., Amphetamine modulates human incentive processing. *Neuron* **43**, 261–269 (2004). doi: 10.1016/j.neuron.2004.06.030; pmid: 15260961
65. D. L. Robinson, B. J. Venton, M. L. Heien, R. M. Wightman, Detecting subsecond dopamine release with fast-scan cyclic voltammetry in vivo. *Clin. Chem.* **49**, 1763–1773 (2003). doi: 10.1373/49.10.1763; pmid: 14500617
66. P. E. Phillips, D. L. Robinson, G. D. Stuber, R. M. Carelli, R. M. Wightman, "Real-time measurements of phasic changes in extracellular dopamine concentration in freely moving rats by fast-scan cyclic voltammetry," in *Drugs of Abuse: Neurological Reviews and Protocols*, J. Q. Wang, Ed. (Methods in Molecular Medicine Series, Humana Press, Totowa, NJ, 2003), pp. 443–464.
67. S. M. Nicola, J. Surmeier, R. C. Malenka, Dopaminergic modulation of neuronal excitability in the striatum and nucleus accumbens. *Annu. Rev. Neurosci.* **23**, 185–215 (2000). doi: 10.1146/annurev.neuro.23.1.185; pmid: 10845063
68. B. Knutson, C. M. Adams, G. W. Fong, D. Hommer, Anticipation of increasing monetary reward selectively recruits nucleus accumbens. *J. Neurosci.* **21**, RC159 (2001). pmid: 11459880
69. B. H. Schott *et al*., Mesolimbic functional magnetic resonance imaging activations during reward anticipation correlate with reward-related ventral striatal dopamine release. *J. Neurosci.* **28**, 14311–14319 (2008). doi: 10.1523/JNEUROSCI.2058-08.2008; pmid: 19109512
70. B. Knutson, S. E. B. Gibbs, Linking nucleus accumbens dopamine and blood oxygenation. *Psychopharmacology* **191**, 813–822 (2007). doi: 10.1007/s00213-006-0686-7; pmid: 17279377
71. H.-S. Liu *et al*., Dorsolateral caudate nucleus differentiates cocaine from natural reward-associated contextual cues. *Proc. Natl. Acad. Sci. U.S.A.* **110**, 4093–4098 (2013). doi: 10.1073/pnas.1207531110; pmid: 23431137
72. G. D. Stuber, T. S. Hnasko, J. P. Britt, R. H. Edwards, A. Bonci, Dopaminergic terminals in the nucleus accumbens but not the dorsal striatum corelease glutamate. *J. Neurosci.* **30**, 8229–8233 (2010). doi: 10.1523/JNEUROSCI.1754-10.2010; pmid: 20554874
73. K. T. Beier *et al*., Circuit architecture of VTA dopamine neurons revealed by systematic input-output mapping. *Cell* **162**, 622–634 (2015). doi: 10.1016/j.cell.2015.07.015; pmid: 26232228
74. N. Lally *et al*., Anti-anhedonic effect of ketamine and its neural correlates in treatment-resistant bipolar depression. *Transl. Psychiatry* **4**, e469 (2014). doi: 10.1038/tp.2014.105; pmid: 25313512
75. G. Juckel *et al*., Dysfunction of ventral striatal reward prediction in schizophrenia. *Neuroimage* **29**, 409–416 (2006). doi: 10.1016/j.neuroimage.2005.07.051; pmid: 16139525
76. E. C. Dowd, D. M. Barch, Anhedonia and emotional experience in schizophrenia: Neural and behavioral indicators. *Biol. Psychiatry* **67**, 902–911 (2010). doi: 10.1016/j.biopsych.2009.10.020; pmid: 20004364
77. A. Lüthi, C. Lüscher, Pathological circuit function underlying addiction and anxiety disorders. *Nat. Neurosci.* **17**, 1635–1643 (2014). doi: 10.1038/nn.3849; pmid: 25402855
78. M. E. Jackson, A. S. Frost, B. Moghaddam, Stimulation of prefrontal cortex at physiologically relevant frequencies inhibits dopamine release in the nucleus accumbens. *J. Neurochem.* **78**, 920–923 (2001). doi: 10.1046/j.1471-4159.2001.00499.x; pmid: 11520912
79. H. E. Covington III *et al*., Antidepressant effect of optogenetic stimulation of the medial prefrontal cortex. *J. Neurosci.* **30**, 16082–16090 (2010). doi: 10.1523/JNEUROSCI.1731-10.2010; pmid: 21123555
80. B. Giros, M. Jaber, S. R. Jones, R. M. Wightman, M. G. Caron, Hyperlocomotion and indifference to cocaine and amphetamine in mice lacking the dopamine transporter. *Nature* **379**, 606–612 (1996). doi: 10.1038/379606a0; pmid: 8628395
81. L. K. Krugel, G. Biele, P. N. Mohr, S.-C. Li, H. R. Heekeren, Genetic variation in dopaminergic neuromodulation influences the ability to rapidly and flexibly adapt decisions. *Proc. Natl. Acad. Sci. U.S.A.* **106**, 17951–17956 (2009). doi: 10.1073/pnas.0905191106; pmid: 19822738
82. Full details of the materials and methods are available as supplementary materials on *Science* Online.
83. G. H. Glover, C. S. Law, Spiral-in/out BOLD fMRI for increased SNR and reduced susceptibility artifacts. *Magn. Reson. Med.* **46**, 515–522 (2001). doi: 10.1002/mrm.1222; pmid: 11550244
84. C. S. Law, G. H. Glover, Interleaved spiral-in/out with application to functional MRI (fMRI). *Magn. Reson. Med.* **62**, 829–834 (2009). doi: 10.1002/mrm.22056; pmid: 19449373
85. C. Chang, G. H. Glover, Variable-density spiral-in/out functional magnetic resonance imaging. *Magn. Reson. Med.* **65**, 1287–1296 (2011). doi: 10.1002/mrm.22722; pmid: 21500257
86. G. T. Buračas, G. M. Boynton, Efficient design of event-related fMRI experiments using M-sequences. *Neuroimage* **16**, 801–813 (2002). doi: 10.1006/nimg.2002.1116; pmid: 12169264
87. G. H. Glover, Deconvolution of impulse response in event-related BOLD fMRI. *Neuroimage* **9**, 416–429 (1999). doi: 10.1006/nimg.1998.0419; pmid: 10191170

ACKNOWLEDGMENTS

We declare no conflicts of interest. K.D. is supported by the Defense Advanced Research Projects Agency Neuro-FAST program; the National Institute of Mental Health; the National Institute on Drug Abuse (NIDA); the NSF; the Simons Foundation; the Gatsby Foundation; the Wiegers Family Fund; and the Grosfeld, Reeves, Snyder, Woo, and Albert Yu and Mary Bechman Foundations. G.H.G. is supported by NIH grant P41 EB015891. This research was also supported in part by a Bio-X Seed grant and a Stanford Neuroscience Institute grant to B.K. and K.D. E.A.F. was supported by a Fulbright International Science and Technology Fellowship, a Stanford Graduate Fellowship, and a Gerald J. Lieberman Fellowship. K.A.Z. was supported by the NSF Graduate Research Fellowship Program, the Stanford Neurosciences Program NIH Training Grant, and a National Research Service Award Predoctoral Fellowship from NIDA (1F31MH105151_01). C.L. was supported by NARSAD and NIH grant R00 MH097822. We thank Z. J. Malchano, T. Davidson, L. J. Pisani, and R. Watkins for advice and technical support and the entire Deisseroth laboratory for guidance. Data displayed in Fig. 6 are available as a full online resource data set at http://clarityresourcecenter.org/ofMRI.html.

SUPPLEMENTARY MATERIALS

www.sciencemag.org/content/351/6268/aac9698/suppl/DC1
Materials and Methods
Figs. S1 to S16
Tables S1 to S7
Caption for Data S1
References (*88*–*95*)

9 July 2015; accepted 17 November 2015
10.1126/science.aac9698